J. Astrophys. Astr. (2018) 39:12
https://doi.org/10.1007/s12036-017-9494-1

Review

Radiatively-driven general relativistic jets

MUKESH K. VYAS and INDRANIL CHATTOPADHYAY*

Aryabhatta Research Institute of Observational Sciences (ARIES), Manora Peak, Nainital 263 002, India.
*Corresponding author. E-mail: indra@aries.res.in

MS received 24 August 2017; accepted 26 October 2017; published online 10 February 2018

Abstract. We use moment formalism of relativistic radiation hydrodynamics to obtain equations of motion of radial jets and solve them using polytropic equation of state of the relativistic gas. We consider curved space-time around black holes and obtain jets with moderately relativistic terminal speeds. In addition, the radiation field from the accretion disc, is able to induce internal shocks in the jet close to the horizon. Under combined effect of thermal as well as radiative driving, terminal speeds up to 0.75 (units of light speed) are obtained.

Keywords. Radiation hydrodynamics—hydrodynamics—shocks—black holes—jets and outflows.

1. Introduction

Jets are ubiquitous in astrophysical objects like active galactic nuclei (AGN e.g., M87), young stellar objects (YSO e.g., HH 30, HH 34), X-ray binaries (e.g., SS433, Cyg X-3, GRS 1915+105, GRO 1655-40), etc.

This paper is devoted to dynamics of relativistic jets around black hole (hereafter BH) candidates like BH X-ray binaries. In such systems, jets can only emerge from accreting matter as BHs neither have hard surface nor are they capable of emission. This fact is supported by strong correlation observed between spectral state of the accretion disc and jet (Fender *et al.* 2010; Gallo *et al.* 2003; Rushton *et al.* 2010). Observations also show that the jet generation region is very close, less than 100 Schwarzschild radii (r_s) around the central object (Junor *et al.* 1999; Doeleman *et al.* 2012). This implies that the entire accretion disc does not take part in jet generation. Following this, we assume that jets are launched within the accretion funnel close to the BH. Further, numerical simulations (Molteni *et al.* 1996; Das *et al.* 2014; Lee *et al.* 2016) and theoretical studies (Chattopadhyay & Das 2007; Das & Chattopadhyay 2008; Chattopadhyay & Kumar 2016; Kumar *et al.* 2013; Kumar & Chattopadhyay 2017) showed that additional thermal gradient term in the accretion corona is able to give rise to bipolar outflows close to the BH.

After the very first theoretical model of accretion discs (Shakura & Sunyaev 1973) being Keplerian in nature, there have been numerous attempts to understand the interaction of radiation with jets (Icke 1980; Sikora & Wilson 1981; Paczyński & Wiita 1980; Fukue 1996; Chattopadhyay & Chakrabarti 2000a, b, 2002; Chattopadhyay *et al.* 2004; Chattopadhyay 2005). Most of these attempts were made considering jets in particle regime while observations reveal their fluid nature. Ferrari *et al.* (1985) studied isothermal and non-radial fluid jets under Newtonian gravity having arbitrary radiation field in special relativistic regime. They obtained mildly relativistic jets and shocks induced by non radial nature of the cross section. Isothermal assumption does not contain the effect of the thermal gradient term which is a significant accelerating agent and is very effective close to the BH. It is also the same region where one needs to consider the effects of general relativity as well. In this series, Vyas *et al.* (2015) studied special relativistic jets under radiation field considering pseudo-Newtonian gravitational potential. They obtained relativistic jets but not multiple sonic points or shock transition. This paper extends the work of Ferrari *et al.* (1985) and Vyas *et al.* (2015) by considering fluid jets in curved space-time. Further, Vyas and Chattopadhyay (2017) showed that non radial jets, even without radiation field do create internal shocks while radial jets do not. Here we explore the possibility that radial jets can form shocks under the impact of sufficiently intense radiation field.

The equations of motion of radiation hydrodynamics were developed by many authors (Hsieh & Spiegel

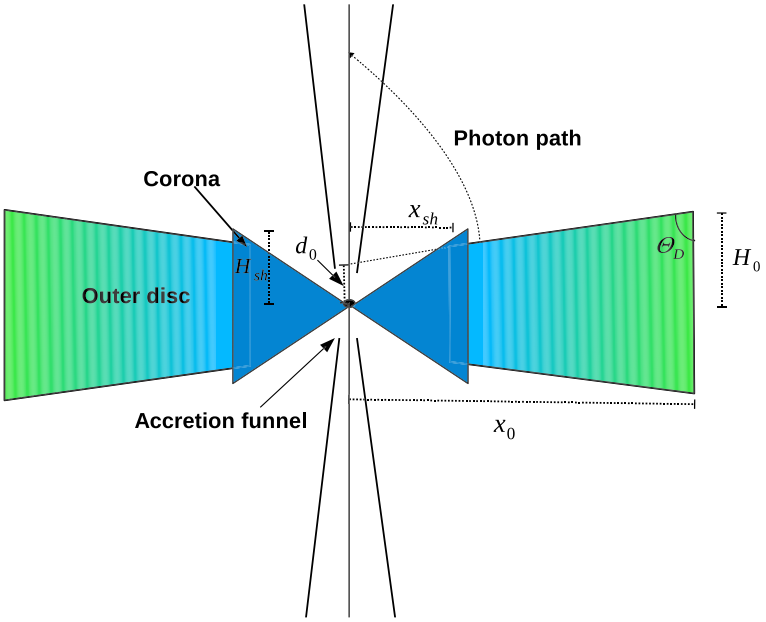

Figure 1. Cartoon diagram of cross-sections of axisymmetric accretion disc and the associated jet in $r,\ \theta, \phi$ coordinates. The outer limit of the corona $x_{\rm sh}$, the intercept of outer disc on the jet axis (d_0), the height of the corona $H_{\rm sh}$ and the outer edge of the disc x_0 are marked.

1976; Mihalas & Mihalas 1984) and later their general relativistic version was obtained in further studies (Park 2006; Takahashi 2007). In this paper we mainly follow the moment formalism to calculate the radiation field above accretion disc (Park 2006).

In section 2, we present assumptions, equations of motion and a brief account of the procedure to compute the radiation field. The methodology to obtain solutions is narrated in section 3. Finally, we present results and draw conclusions in section 4

2. Assumptions and governing equations

2.1 *Assumptions*

We invoke general relativity to take care of space-time curvature, which around a non-rotating BH is described by Schwarzschild metric as

$$\begin{aligned} {\rm d}s^2 &= -g_{tt}c^2{\rm d}t^2 + g_{rr}{\rm d}r^2 + g_{\theta\theta}{\rm d}\theta^2 + g_{\phi\phi}{\rm d}\phi^2 \\ &= -\left(1-\frac{2GM_{\rm B}}{c^2r}\right)c^2{\rm d}t^2 + \left(1-\frac{2GM_{\rm B}}{c^2r}\right)^{-1}{\rm d}r^2 \\ &\quad + r^2{\rm d}\theta^2 + r^2\sin^2\theta{\rm d}\phi^2. \end{aligned} \tag{1}$$

Here r, θ and ϕ are the usual spherical coordinates, t is the time, $g_{\mu\mu}$ are the diagonal metric components, $M_{\rm B}$ is the mass of the central black hole and G is the universal constant of gravitation. Hereafter, we use geometric units (unless specified otherwise) with $G = M_{\rm B} = c = 1$ with the units of mass, length and time being $M_{\rm B}$, $r_{\rm g} = GM_{\rm B}/c^2$ and $t_{\rm g} = GM_{\rm B}/c^3$ respectively for which, the event horizon is at $r_{\rm S} = 2$. The jet is assumed to be in steady state (i.e., $\partial/\partial t = 0$) and as the relativistic jets are collimated, we consider on-axis (i.e., $u^r = u^\phi = \partial/\partial r = 0$) and axis-symmetric ($\partial/\partial\phi = 0$) jets with small opening angle. Narrow jet allows us to further assume that at distance r, the physical variables of the jet remain same along its breadth. The jet is assumed to expand radially, perpendicular to the accretion plane. Further, a jet should have low angular momentum else it cannot remain collimated and following the effective angular momentum removal by radiation and magnetic fields, we assume jets to be non-rotating. The cartoon diagram of disc jet system is shown in Fig. 1. The accretion disc has an outer disc and the inner torus like corona. The outer edge of the corona and the inner edge of the outer disc is presented by $x_{\rm sh}$. The height of the corona is assumed to be $H_{\rm sh} = 2.5x_{\rm sh}$. Accretion disc works as a source of radiation emitting via synchrotron, bremsstrahlung and inverse Compton processes along with the assumption that magnetic pressure in the disc is a fraction β of the gas pressure. We take $\beta = 0.5$ in this paper. To compute the radiation from the disc, the density, velocity and the temperature distribution of the accretion disc has to be estimated. We follow the methods of Vyas *et al.* (2015) to obtain an analytical estimate of the flow variables in the accretion

disc. We do not consider how the jets are being launched from the jet. The accretion disc plays an auxiliary role only. The plasma is assumed to be fully ionized and the interaction between radiation and matter is dominated by Thomson scattering. In the scattering regime only momentum is transferred between radiation, and matter and energy transfer does not take place. The relativistic effects on radiation field observed are also incorporated. The relativistic effects in the radiative transfer explicitly appears in the equations of motion while the effects of photon bending in radiation field are approximated taking the help of Beloborodov (2002) and Bini *et al.* (2015). Beloborodov's (2002) analysis approximated transformed radiation field due to curved space-time which is close to the exact values. The transformation of flat space-time relativistic specific intensities (I_{j_f}) into curved space-time are given as

$$I_j = I_{j_f}\left(1-\frac{2}{r_\mathrm{a}}\right)^2. \tag{2}$$

Here r_a is the radial coordinate of the source point on the accretion disc. The suffix $j \rightarrow \mathrm{OD},\ \mathrm{C}$ signifies the contribution from the outer disc and the corona, respectively. The square of redshift factor $(1-2/r_\mathrm{a})$ shows that curved space-time reduces the observed intensity.

Further, as photon moves in a curved path, the transformed expressions of the direction cosine and solid angle are given in terms of their flat space counterparts as (Beloborodov 2002)

$$\begin{aligned} l_j &= l_{jf}\left(1-\frac{2}{r_\mathrm{a}}\right)+\frac{2}{r_\mathrm{a}},\\ \mathrm{d}\Omega_j &= \left(1-\frac{2}{r_\mathrm{a}}\right)\mathrm{d}\Omega_{jf}. \end{aligned} \tag{3}$$

Using these transformation laws, the radiative moments namely radiation energy density (R_0), radiation flux (R_1), radiation pressure (R_2) and disc luminosities are calculated using similar procedure as in Vyas *et al.* (2015). Here we have excluded radiation contribution from Keplerian disc as its contribution in the various components of total radiative moments was found to be negligible. The luminosity of the outer disc is obtained by integrating specific intensities over the disc surface and then using the luminosity ratio relation between the outer disc and the corona (Vyas *et al.* 2015) for $M_\mathrm{B} = 10M_\odot$, we obtain luminosities of the corona. The total luminosity (ℓ) of the disc then is an addition of both the luminosities and is shown in units of Eddington luminosity in this paper. We treat ℓ as an input parameter.

2.2 *Governing equations*

2.2.1. *Equation of state.* Equation of state (EoS) is a closure relation between internal energy density (e), pressure (p) and mass density (ρ) of the fluid. In this study, we consider the jet fluid obeying polytropic EoS having fixed adiabatic index ($\Gamma = 1.5$) given as

$$e = \rho + \frac{p}{\Gamma - 1}. \tag{4}$$

Expressions for adiabatic sound speed a in relativistic regime and enthalpy h are given by

$$a^2 = \frac{\Gamma p}{e+p} = \frac{\Gamma\Theta}{1+N\Gamma\Theta};\quad h = \frac{e+p}{\rho} = 1+\Gamma N\Theta. \tag{5}$$

Here $N(=\frac{1}{\Gamma-1}=2)$ is the polytropic index of the flow and non-dimensional temperature is defined as $\Theta = p/\rho$.

2.2.2. *Dynamical equations of motion.* In relativistic notation, the equations of motion of any system are obtained when the four divergence of the energy-momentum tensor $T^{\alpha\beta} = T_\mathrm{R}^{\alpha\beta} + T_\mathrm{M}^{\alpha\beta}$ is set to zero, i.e.,

$$T^{\alpha\beta}_{;\beta} = (T_\mathrm{R}^{\alpha\beta} + T_\mathrm{M}^{\alpha\beta})_{;\beta} = 0. \tag{6}$$

Here, $T_\mathrm{R}^{\alpha\beta}$ and $T_\mathrm{M}^{\alpha\beta}$ stand for jet matter and radiation field respectively and are given by (Mihalas & Mihalas 1984)

$$T_\mathrm{M}^{\alpha\beta} = (e+p)u^\alpha u^\beta + pg^{\alpha\beta};\quad T_\mathrm{R}^{\alpha\beta} = \int I_\nu l^\alpha l^\beta \mathrm{d}\nu\mathrm{d}\Omega. \tag{7}$$

The metric tensor components are given by $g^{\alpha\beta}$, u^α which are the components of four velocity, e and p the fluid energy density and pressure in the local co-moving frame. Furthermore, l^α are the directional derivatives, I_ν the specific intensity of the radiation field with ν being the frequency of the radiation. Ω is the solid angle subtended by a source point at the accretion disc surface on to the field point at the jet axis.

In the absence of particle creation/destruction, conservation of four mass-flux is given by

$$(\rho u^\beta)_{;\beta} = 0, \tag{8}$$

where ρ is the mass density of the fluid. From the above, the set of equations (equation (6)) and the momentum balance equation in the i-th direction is obtained using projection tensor, $(g^i_\alpha + u^i u_\alpha)$ i.e.,

$$(g^i_\alpha + u^i u_\alpha)T^{\alpha\beta}_{\mathrm{M};\beta} = -(g^i_\alpha + u^i u_\alpha)T^{\alpha\beta}_{\mathrm{R};\beta}. \tag{9}$$

For an on-axis jet in the steady state it becomes (Park 2006)

$$u^r\frac{\mathrm{d}u^r}{\mathrm{d}r}+\frac{1}{r^2}=-\left(1-\frac{2}{r}+u^ru^r\right)\frac{1}{e+p}\frac{\mathrm{d}p}{\mathrm{d}r}+\frac{\rho_\mathrm{e}\sigma_\mathrm{T}}{m_\mathrm{p}(e+p)}\Im^r, \tag{10}$$

Here ρ_e is the lepton mass density, m_p is the mass of the proton and $\Im^r$ is the net radiative contribution and is given by

$$\Im^r=\sqrt{g^{rr}}\gamma^3\left[(1+v^2)R_1-v\left(g^{rr}R_0+\frac{R_2}{g^{rr}}\right)\right]. \tag{11}$$

Here we define three velocity v of the jet as

$$v^2=-u_iu^i/u_tu^t=-u_ru^r/u_tu^t\Longrightarrow u^r=\gamma v\sqrt{g^{rr}}$$

and $\gamma^2=-u_tu^t$ is the Lorentz factor. R_0, R_1 and R_2 are zeroth, first and second moments of specific intensity. Similarly, the energy conservation equation is obtained by taking

$$u_\alpha T^{\alpha\beta}_{\mathrm{M};\beta}=-u_\alpha T^{\alpha\beta}_{\mathrm{R};\beta}. \tag{12}$$

In the scattering regime, it becomes

$$\frac{\mathrm{d}e}{\mathrm{d}r}-\frac{e+p}{\rho}\frac{\mathrm{d}\rho}{\mathrm{d}r}=0. \tag{13}$$

The absence of emission/absorption makes the right side of equation (13) as zero. It is a consequence of scattering regime assumption and shows that the system is isentropic. From continuity equation (equation (14)), the mass outflow rate is given as

$$\dot{M}_\mathrm{out}=\Omega\rho u^r r^2;\quad \Omega=\text{geometric constant}. \tag{14}$$

The differential form of the outflow rate equation is

$$\frac{1}{\rho}\frac{\mathrm{d}\rho}{\mathrm{d}r}=-\frac{2}{r}-\frac{1}{u^r}\frac{\mathrm{d}u^r}{\mathrm{d}r}. \tag{15}$$

Equation (13) can be integrated with the help of equation (4) to obtain isentropic relation between p and ρ as

$$p=k\rho^\Gamma,$$

where k is the entropy constant of the flow. This equation enable us to replace ρ from equation (14), and we obtain the expression for entropy-outflow rate as

$$\dot{\mathcal{M}}=\Theta^N u^r r^2. \tag{16}$$

$\dot{\mathcal{M}}$ remains constant along the streamline of the jet, except at the shock.

Integrating equation (10), we obtain generalized, relativistic Bernoulli parameter for the radiatively-driven jet,

$$E=-hu_t\exp\left(\int\mathrm{d}r\frac{\sigma_\mathrm{T}(1-Na^2)\Im^r}{m_\mathrm{p}\gamma^2(1-2/r)}\right). \tag{17}$$

The momentum balance equation (equation (10)), with the help of equation (15), is simplified to

$$\gamma^2vg^{rr}r^2\left(1-\frac{a^2}{v^2}\right)\frac{\mathrm{d}v}{\mathrm{d}r}=a^2(2r-3)-1+\frac{\Im^r r^2(1-Na^2)}{m_\mathrm{p}\gamma^2}. \tag{18}$$

Using energy conservation equation (13) along with the EoS (equation (4)), the expression of temperature gradient along r is obtained as

$$\frac{\mathrm{d}\Theta}{\mathrm{d}r}=-\frac{\Theta}{N}\left[\frac{\gamma^2}{v}\left(\frac{\mathrm{d}v}{\mathrm{d}r}\right)+\frac{2r-3}{r(r-2)}\right]. \tag{19}$$

Equations (6) and (8), the two equations of motion reduce to two differential equations (18) and (19), which describes the distribution of two flow variables v and Θ.

3. Methods of analysis

The solution for radiatively-driven jet can be obtained if equations (18) and (19) are solved. Since jets are launched from the accretion disc, close to the central object, the injection speed will be small, while the temperature will be high. So at the base, jets should be subsonic. Far away from the base, jets are observed to be moving with relativistic speed and therefore supersonic. Hence such flows are transonic in nature. The distance ($r=r_\mathrm{c}$) at which the bulk speed ($v=v_\mathrm{c}$) crosses the local sound speed ($a=a_\mathrm{c}$), is called the sonic point. Equation (18) shows that the sonic point is also a critical point since at $r=r_\mathrm{c}$, $\mathrm{d}v/\mathrm{d}r\to 0/0$. This property gives the sonic or critical point conditions as

$$v_\mathrm{c}=a_\mathrm{c} \tag{20}$$

and

$$a_\mathrm{c}^2(2r_\mathrm{c}-3)-1+\frac{\Im^r_\mathrm{c}r_\mathrm{c}^2(1-N_\mathrm{c}a_\mathrm{c}^2)}{m_\mathrm{p}\gamma_\mathrm{c}^2}=0. \tag{21}$$

Here c denotes that the values are obtained at the sonic point ($r=r_\mathrm{c}$). For a given r_c, we solve equation (21) to find a_c and then Θ_c (equation (5)). We can also compute $\dot{\mathcal{M}}_\mathrm{c}$, E_c at r_c (using equations (16) and (17)). Since $E_\mathrm{c}=E$ for a particular solution, therefore, for a given E, r_c is determined and vice versa. In other words, sonic point is a mathematical boundary. So we first obtain all the variables at r_c and then calculate $|\mathrm{d}v/\mathrm{d}r|_\mathrm{c}$ by using the L'Hospital's rule in equation (18) at $r=r_\mathrm{c}$.

This leads to a quadratic equation for $|\mathrm{d}v/\mathrm{d}r|_c$, which can admit two complex roots having 'spiral' type sonic points, or two real roots but with opposite signs (called X or 'saddle' type sonic points), or real roots with the same sign (known as nodal type sonic point). For a given boundary value at the base of the jet ($r = r_b = 3$) the transonic solutions will pass through sonic points determined by E and $\dot{\mathcal{M}}$ of the flow giving the values at the outer boundary r_∞ (defined by $r = r_\infty = 10^5$). We integrate equations (18) and (19) simultaneously inward and outward from r_c using the 4-th order Runge-Kutta method.

3.1 *Shock conditions*

The existence of multiple sonic points in the flow opens up the possibility of formation of shocks in the flow. At the shock, the flow is discontinuous in density, pressure and velocity. The relativistic Rankine–Hugoniot conditions relate the flow quantities across the shock jump (Chattopadhyay & Chakrabarti 2011)

$$[\rho u^r] = 0, \tag{22}$$

$$[\dot{E}] = 0 \tag{23}$$

and

$$[T^{rr}] = [(e + p)u^r u^r + pg^{rr}] = 0. \tag{24}$$

The square brackets denote the difference of quantities across the shock, i.e. $[Q] = Q_2 - Q_1$ with Q_2 and Q_1 being the quantities after and before the shock respectively.

Equation (23) states that the energy flux remains conserved across the shock. Dividing (24) by (22) and a little algebra leads to

$$(1 + \Gamma N\Theta)u^r + \Theta g^{rr} = 0. \tag{25}$$

We check for shock conditions equations (23) and (25) as we solve the equations of motion of the jet.

4. Results and discussion

4.1 *Nature of radiation field*

In Fig. 2, we show radiative moments R_0 (solid, black), R_1 (long-dashed, blue) and R_2 (red, dashed) as functions of r calculated at the jet axis for $\dot{m} = 9.145$ which corresponds to $x_{sh} = 14.67$ and $\ell = 0.5$. The first peak ($\lesssim$10) in the moments, is due to the radiation from the corona, and the second peak (55) is due to the radiation from the outer disc. Due to the shadow effect from the post-shock disc, all moments from the outer disc

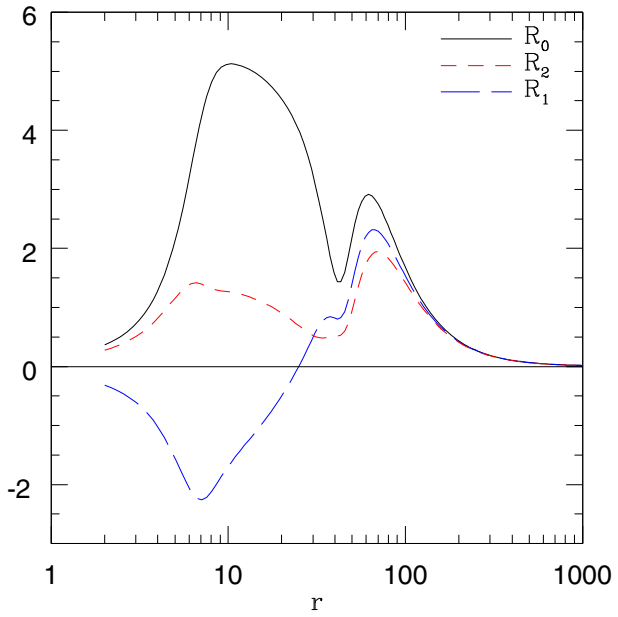

Figure 2. Radiative moments R_0, R_1 and R_2 from the accretion disc corresponding to accretion rate ($\dot{m}$) to be 9.145 or disc luminosity (ℓ) to be 0.5. Both $\dot{m}$ and ℓ are in Eddington units.

are zero for $r < 30$. Since the corona is geometrically thick, the radiative flux R_1 is negative in the funnel-like region. The magnitude of the moments rise as the jet sees more of the disc as it propagates upward and they decay after reaching a peak value. The moments follow an inverse square-law at large distances. The negative flux in the funnel pushes the jet material downward and works against the motion, to the extent that, it may drive shock in jets.

4.2 *Nature of sonic points and behaviour of flow variables*

Using the procedure explained in section 3, we provide sonic point r_c and calculate physical variables. In Figures 3(a), (b) and (c), we show variation of Θ_c, $\dot{\mathcal{M}}_c$ and a_c with r_c, respectively. Various curves are plotted for different luminosities as $\ell = 2.85$ (dotted, black), 1.76 (dashed, blue), 0.80 (long-dashed, red), 0.035 (dashed-dotted, magenta) and all these are compared with the thermal flow $\ell = 0.00$ (solid, black). Physically different sonic points mean different choices of boundary conditions that give different transonic solutions. Similarly, choice of an r_c implies a solution with an unique choice of E and $\dot{\mathcal{M}}$. For all possible values of r_c, thermal jets harbour real roots of a_c (or, corresponding Θ_c), while radiation field limits the region where a_c can have

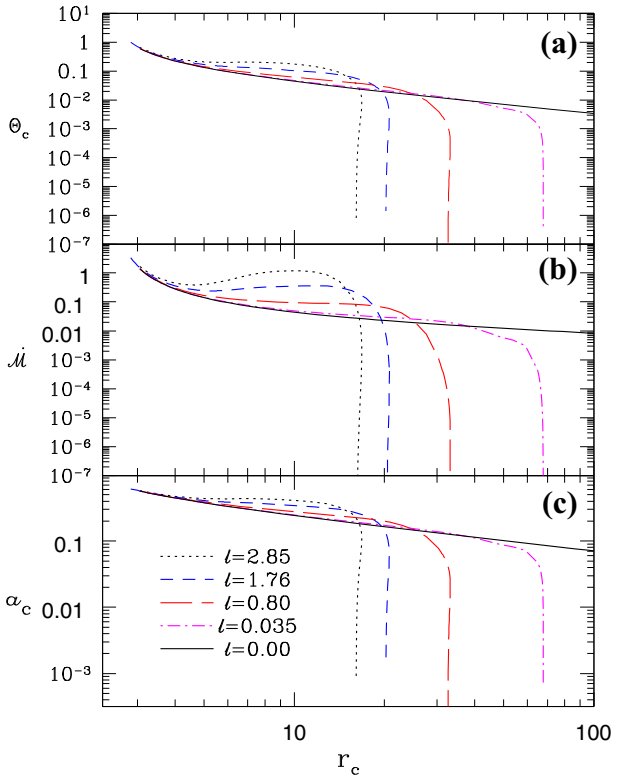

Figure 3. Variation of Θ_c (**a**), $\dot{\mathcal{M}}_c$ (**b**) and a_c (**c**) with r_c for various values of ℓ.

real values. For $r_c > r_{c_{max}}$, one obtains complex values of a_c (equation (21)). It is also found that $r_{c_{max}}$ always lies inside the corona funnel (i.e., $r_{c_{max}} < H_{sh}$). Physically, the critical points where a_c is found imaginary, correspond to solutions where fluid approximation breaks down or physical temperatures are not defined.

In Fig. 4, we show a typical nature of flow variables along r for $\ell = 0.8$ and $E = 1.43$. In Fig. 4(a), we show variation of three velocity v (solid, black) and a (long-dashed, blue). The effect of negative flux is clearly seen as v decreases inside the funnel and then it accelerates above it. In Fig. 4(b), we plot the entropy outflow rate $\dot{\mathcal{M}}$ which remains constant since scattering is an isentropic process. Figure 4(c) shows a sharp decline of temperature due to adiabatic expansion. In Fig. 4(d), we compare v of radiatively-driven jet (solid, black), and thermally-driven solution (dashed, red), both having the same E. We see that radiative acceleration dominates over radiative drag and terminal speed of the jet is higher in the presence of radiation field.

Now in Figures 5(a)–(d), we investigate behaviour of jet speeds with different boundary conditions, i.e., different choices of E. We choose $\ell = 1.76$ and plot E_c with r_c in Fig. 5(a). For very high values of $E = E_c = 1.83$ the flow is hot, and radiation is in-effective (Fig. 5(b)). The jet accelerates due to the thermal gradient term and becomes transonic at $r_c = 3.2$. As the jet expands, the temperature decreases and radiation becomes effective. The combined effect of negative flux in the funnel and radiation drag term decelerates the speed. Above the funnel radiation flux becomes positive and starts to accelerate the jet and it achieves terminal speed of $v_T = 0.76$. If one chooses lower values of $E = 1.33$ (Fig. 5(c)), the jet passes through the inner sonic point at $r = 4.4$. Because the energy is low, radiation is more effective. Radiation flux opposes the outflowing jet inside the funnel more vigorously and causes a shock transition — a discontinuous transition from supersonic branch to subsonic branch at $r = 6.78$ and then after coming out of the accretion funnel, it again accelerates under radiation push and becomes transonic, forming an outer sonic point at $r = 14.77$. The terminal speed achieved for this case is ∼0.7. Here the jet crosses two sonic points with $\dot{\mathcal{M}}$ to be higher for outer sonic point ($\dot{\mathcal{M}} = 0.291$) than the inner one ($\dot{\mathcal{M}} = 0.287$). Vyas and Chattopadhyay (2017) showed that conical jets without radiation do not form shock, but here we see that radiation field is able to induce shocks in radially outflowing jets. For even lower energy $E = 1.01$ (Fig. 5(d)), the radiation is even more effective, and the jet speed is drastically reduced within the funnel. However, above the funnel it is accelerated very efficiently, becoming transonic through a single sonic point and achieves terminal speed of about $v_T \sim 0.65$.

We now choose low energy jets, whose base speeds are very low (similar to Fig. 5(d)). Since these jets have very low base speeds and base temperatures, we use them to compare jet speeds acted on by various disc luminosities. In Fig. 6(a), we compare v with r for $\ell = 2.85$ (solid, black), $\ell = 1.76$ (dotted, black), $\ell = 0.80$ (red, dashed) and $\ell = 0.21$ (long-dashed, magenta). We observe that higher radiation accelerates the jets up to greater speeds. In Fig. 6(b), we plot the terminal speed (v_T) as a function of ℓ. The base speed of these jets are very low. For super Eddington luminosities, like $\ell = 2.85$, the jet achieves terminal speeds to be around 0.75.

4.2.1. *Effect of corona geometry, magnetic pressure in disc* (β) *and* Γ. In this paper, we have considered thick discs with corona height being 2.5 times its width. One may wonder how the results would behave if discs are less thicker. To compare the effects of different geometries, we choose $H_{sh} = 0.6x_{sh}$ as in Vyas *et al.* (2015) and generate velocity profiles of the jet for $\ell = 1.76$ and $E = 1.33$ (same parameters as in Fig. 5(c)). The profiles are plotted in Fig 7(a) for

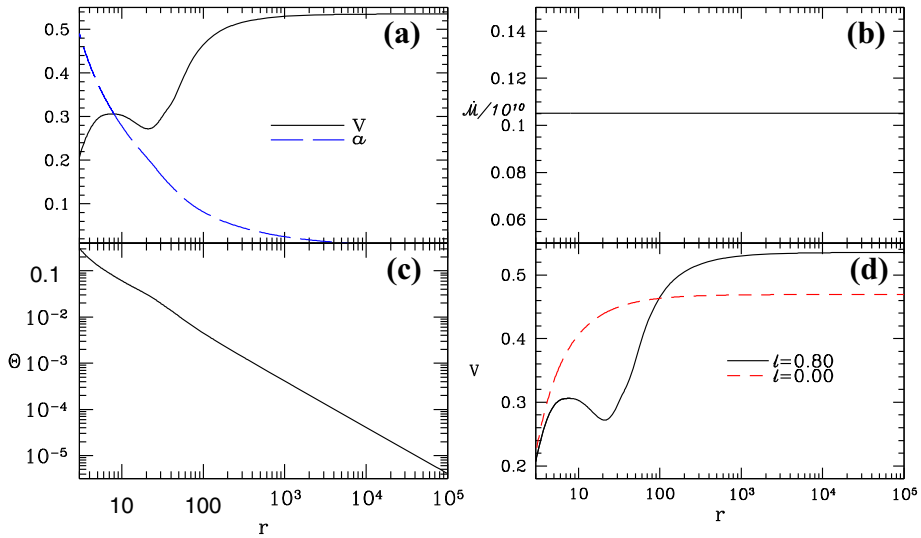

Figure 4. (**a**) Variation of three velocity v (solid black) and a (long-dashed blue), (**b**) $\dot{\mathcal{M}}$, and (**c**) Θ with r for $\ell = 0.80$. (**d**) Comparison of v for $\ell = 0.8$ (solid black) with v for $\ell = 0$ (red dashed). For all the plots, $E = 1.43$.

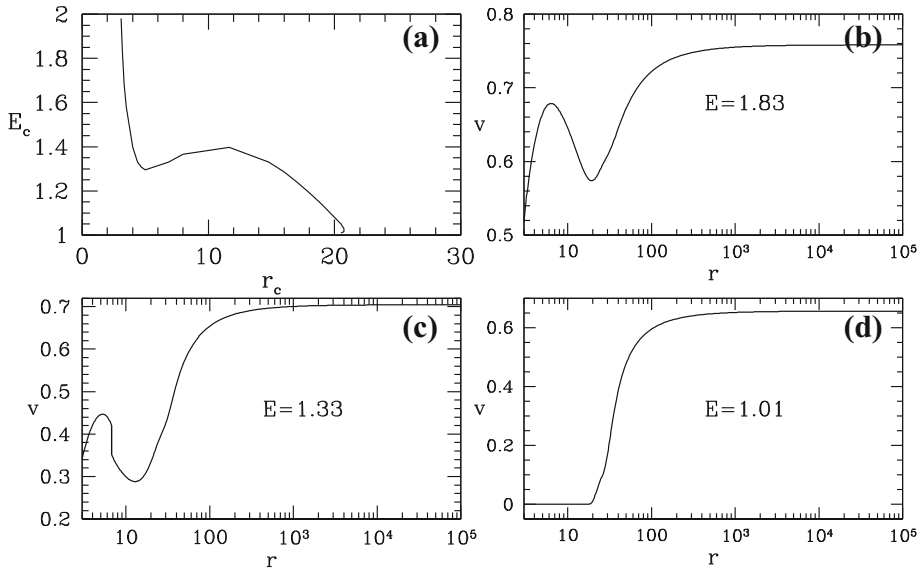

Figure 5. (**a**) Variation of E_c with r_c; variation of v with r for (**b**) $E = 1.83$, (**c**) $E = 1.33$ and (**d**) $E = 1.01$. For all the curves, $\ell = 1.76$.

thicker ($H_{sh} = 2.5x_{sh}$, solid, black) and thinner corona ($H_{sh} = 0.6x_{sh}$, dashed, red). It is clear that radiation from geometrically thick corona is more capable to produce a shock, as the jet faces negative flux after being launched. For thinner corona, the radiation resistance is relatively less and the jet is unable to form a shock inside the funnel. Further, lesser resistance inside the funnel of thinner disc, makes radiative acceleration more effective and as a result the terminal speed is greater.

The choice of the value of Γ is a tricky issue. This is because the base of the jet is hot and Γ should be closer to, but not exactly 4/3 (Chattopadhyay & Ryu 2009). And it should be lower than 5/3, therefore, we took the median value of 1.5 in the previous sections. If one considers different values of Γ, then the behaviour of the jet changes because, different choices of Γ alters the net heat content of the flow. In Fig. 7(b), we plot v_T as a function of E for $\ell = 0.80$ and $\Gamma(= 1.4$, solid black), $\Gamma(= 1.5$, red dashed) and $\Gamma(= 1.6$, long dashed magenta). Smaller value of Γ results in higher thermal driving and produces faster jets.

In this study, β parameter is introduced to compute the synchrotron cooling from stochastic magnetic field. Therefore in steady state, it is most likely that $\beta < 1$, otherwise steady disc will not form. We took $\beta = 0.5$ as an ad hoc value. Increasing

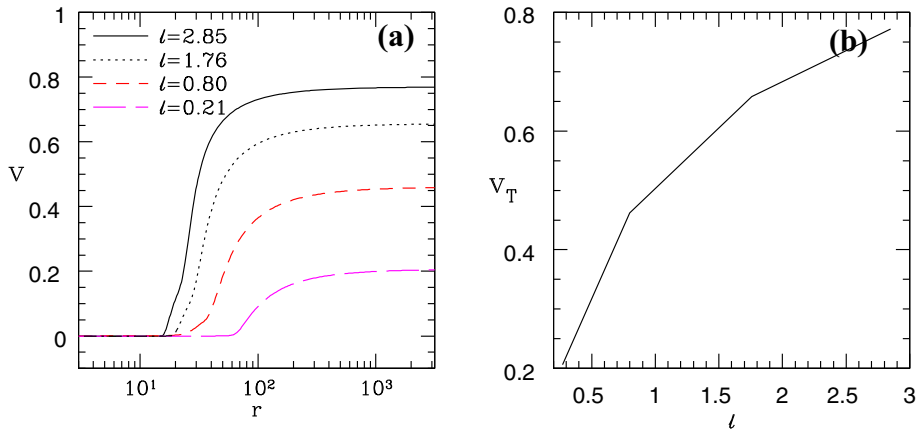

Figure 6. (**a**) Variation of v with r for various luminosities ranging from $\ell = 0.21$ to 2.85. (**b**) v_T as a function of ℓ.

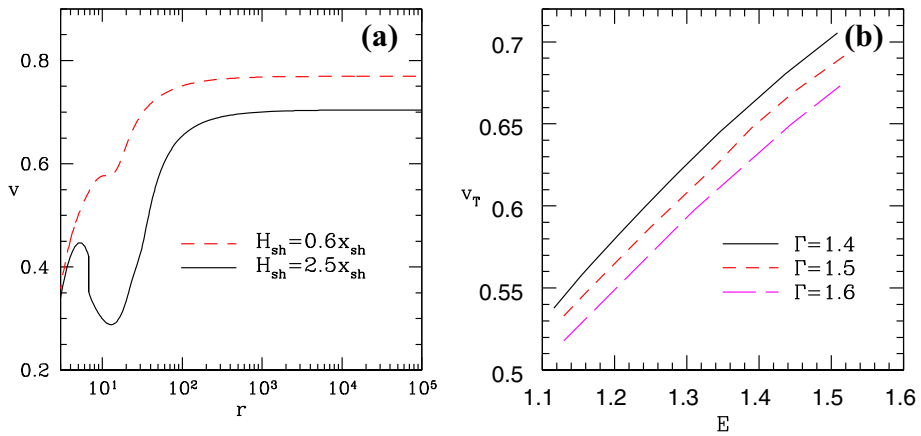

Figure 7. **(a)** Variation of v with r for various disc height ratios, $H_{sh} = 2.5x_{sh}$ (solid black) and $H_{sh} = 0.6x_{sh}$ (red dashed) for $\ell = 1.76$. **(b)** v_T as a function of E for varying Γ keeping $\ell = 0.80$.

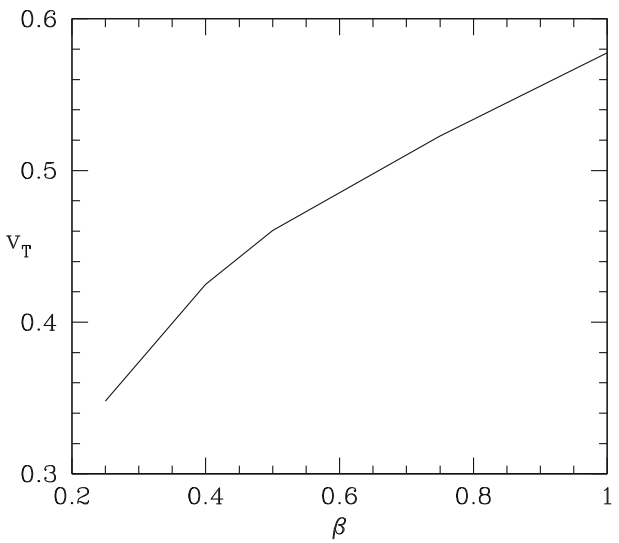

Figure 8. v_T is plotted as a function of β, for $\dot{m} = 10$ and $H_{sh} = 2.5x_{sh}$.

β would increase synchrotron radiation, but would not increase bremsstrahlung because $\dot{m}$ is not being changed. Moreover, the number of hot electrons which inverse-Comptonize soft photons also do not change much, although increasing β amounts to increasing ℓ, the distribution of ℓ is different and therefore, the response of v_T to β is different than $\dot{m}$ or ℓ, as was shown in Vyas *et al.* (2015). Figure 8 shows the variation of v_T as a function of β for a given $\dot{m}$ and $H_{sh} = 2.5x_{sh}$.

4.3 *Final remarks*

This paper is development and expansion of earlier papers on radiatively-driven fluid jets (Ferrari *et al.* 1985; Chattopadhyay & Chakrabarti 2002; Vyas *et al.* 2015). While the previous papers are either in Newtonian or special relativistic regimes, the present effort is in general relativistic regimes. Only Ferrari *et al.* (1985) showed the presence of radiatively-driven shocks in

jets, but the terminal speeds were pitiable. Most likely, the low terminal speeds are a result of their preference of isothermal approximation. Even though the details of accretion disc physics have been ignored, but still broad geometric features like a thicker corona and outer flatter disc, produced a significantly different radiative moment distribution, which resulted in a set of very rich classes of jet solutions.

References

Beloborodov A. M. 2002, ApJ, 566, L85

Bini D., Geralico A., Jantzen R. T., Semerak O. 2015, MNRAS, 446, 2317

Chattopadhyay I., Chakrabarti S. K. 2000a, Int. J. Mod. Phys. D, 9, 57

Chattopadhyay I., Chakrabarti S. K. 2000b, Int. J. Mod. Phys. D, 9, 717

Chattopadhyay I., Chakrabarti S. K. 2002, MNRAS, 333, 454

Chattopadhyay I., Das S., Chakrabarti S. K. 2004, MNRAS, 348, 846

Chattopadhyay I., Chakrabarti S. K. 2011, Int. J. Mod. Phys. D, 20, 1597

Chattopadhyay I. 2005, MNRAS, 356, 145

Chattopadhyay I., Das S. 2007, New A, 12, 454

Chattopadhyay I., Kumar R. 2016, MNRAS, 459, 3792

Das S., Chattopadhyay I. 2008, New A, 13, 549

Das S., Chattopadhyay I., Nandi A., Molteni D. 2014, MNRAS, 442, 251

Doeleman S. S. *et al.* 2012, Science, 338, 355

Fender R. P., Gallo E., Russell D. 2010, MNRAS, 406, 1425

Ferrari A., Trussoni E., Rosner R., Tsinganos K. 1985, ApJ, 294, 397

Fukue J. 1996, PASJ, 48, 631

Gallo E., Fender R. P., Pooley G. 2003, MNRAS, 344, 60

Hsieh H. S., Spiegel E. A. 1976, ApJ, 207, 244

Icke V. 1980, AJ, 85, 329

Junor W., Biretta J. A., Livio M. 1999, Nature, 401, 891

Kumar R., Chattopadhyay I. 2017, MNRAS, 469, 4221

Kumar R., Singh C. B., Chattopadhyay I., Chakrabarti S. K. 2013, MNRAS, 436, 2864

Chattopadhyay I., Ryu D. 2009, ApJ, 694, 492

Lee S.-J., Chattopadhyay I., Kumar R., Hyung S., Ryu D. 2016, ApJ, 831, 33

Mihalas D., Mihalas B. W. 1984, Foundations of Radiation Hydrodynamics Oxford University Press, Oxford

Molteni D., Ryu D., Chakrabarti S. K. 1996, ApJ, 470, 460

Park M.-G. 2006, MNRAS, 367, 1739

Paczyński B., Wiita P. J. 1980, A&A, 88, 23

Rushton A., Spencer R., Fender R., Pooley G. 2010, A&A, 524, 29

Shakura N. I., Sunyaev R. A. 1973, A&A, 24, 337S

Sikora M., Wilson D. B. 1981, MNRAS, 197, 529

Takahashi R. 2007, MNRAS, 382, 1041

Vyas M. K., Kumar R., Mandal S., Chattopadhyay I. 2015, MNRAS, 453, 2992

Vyas M. K., Chattopadhyay I. 2017, MNRAS, 469, 3270